Remote Sensing of Environment 133 (2013) 52–61

Contents lists available at SciVerse ScienceDirect

Remote Sensing of Environment

journal homepage: www.elsevier.com/locate/rse

Using field spectroscopy to assess the potential of statistical approaches for the retrieval of sun-induced chlorophyll fluorescence from ground and space

Luis Guanter [a,*], Micol Rossini [b], Roberto Colombo [b], Michele Meroni [c], Christian Frankenberg [d], Jung-Eun Lee [d], Joanna Joiner [e]

[a] Institute for Space Sciences, Free University of Berlin, Germany
[b] Remote Sensing of Environmental Dynamics Laboratory, DISAT, Università degli Studi Milano-Bicocca, Italy
[c] European Commission, DG-JRC, Institute for Environment and Sustainability, Ispra, Varese, Italy
[d] Jet Propulsion Laboratory, California Institute of Technology, Pasadena, USA
[e] NASA Goddard Space Flight Center, Greenbelt, MD, USA

ARTICLE INFO

Article history:
Received 22 June 2012
Received in revised form 23 January 2013
Accepted 25 January 2013
Available online xxxx

Keywords:
Fluorescence retrieval
Fraunhofer-line approach
GOSAT-FTS
Singular vector decomposition
O_2A-band

ABSTRACT

Sun-induced chlorophyll fluorescence (F_s) is an electromagnetic signal emitted in the 650–800 nm spectral window by the chlorophyll-*a* of green leaves. Previous studies demonstrated the retrieval of F_s on a global scale using high spectral resolution measurements by the Fourier Transform Spectrometer (FTS) on board the greenhouse gases observing satellite (GOSAT). The retrieval of F_s from GOSAT-FTS data is based on the modeling of the in-filling of solar Fraunhofer lines by F_s. The first F_s retrieval methods for GOSAT-FTS measurements were based on physical formulations of the radiative transfer between the atmosphere, the surface and the instrument including the F_s emission. As an alternative, a statistical method was also successfully applied to GOSAT data. This method is based on a singular vector decomposition (SVD) technique producing a basis of spectral functions able to model the contribution of the reflected solar radiation to the top-of-atmosphere measurement in a linear way. The F_s signal is included in the forward model as an extra parameter adding to the reflected solar radiation. Here, we use field spectroscopy measurements to provide further experimental evidence on the retrieval of F_s with statistical approaches in both Fraunhofer lines and atmospheric oxygen and water vapor bands. The statistical retrieval method used with GOSAT-FTS data has been adapted to a set of ground-based spectro-radiometer measurements in the 717–780 nm range. Retrieval results in the 745–759 nm window, which contains only Fraunhofer lines, support the overall approach of estimating F_s from space measurements in that spectral window. Furthermore, the application of the method to broader fitting windows including both Fraunhofer lines and and (oxygen and water vapor) atmospheric bands atmospheric bands has been proven to be very effective to reduce the retrieval noise and has also shown a good comparison with reference O_2A-based retrievals. This allows consideration of statistical methods as a powerful option for F_s retrieval from broad-band space-based measurements in the near-infrared.

1. Introduction

A small fraction (~1%) of the solar radiation absorbed by green leaves is emitted as chlorophyll-*a* fluorescence, which is widely known as sun-induced chlorophyll fluorescence (F_s). The F_s emission spectrum expands from around 650 nm to over 800 nm and includes two broad-band peaks centered in the red (685 nm) and far-red (740 nm) spectral regions (e.g. Baker, 2008). Because F_s and photochemistry compete for excitation energy in photosystem II (the photosystem where most of the fluorescence emanates from), the F_s signal is widely regarded as a potential tool to track changes in photosynthetic activity of vegetation via remote sensing (Daumard et al., 2010; Flexas et al., 2002; Porcar-Castell, 2011; Soukupová et al., 2008).

Even though there has been an intense activity in the field of the remote sensing of sun-induced chlorophyll fluorescence in the last years (Meroni et al., 2009, and references therein), it has not been until very recently that measurements of s from space have been proven feasible (Guanter et al., 2007) and the first global maps of F_s have been produced (Frankenberg et al., 2011b; Guanter et al., 2012; Joiner et al., 2011, 2012). The initial analysis of those maps has shown a high correlation between F_s and gross primary production at the global and regional scales (Frankenberg et al., 2011b; Guanter et al., 2012). This can represent a decisive step towards the global mapping of photosynthesis from space.

The main challenge for F_s retrieval is to disentangle it from the solar signal reflected by the atmosphere and the surface. At the ground level, this has been achieved with high spectral resolution measurements in the 600–800 nm window and the modeling of the *in-filling* of the O_2A-band by F_s. This modeling has traditionally relied on the Fraunhofer Line Discriminator (FLD) principle (Alonso et al.,

* Corresponding author. Tel.: +49 30 83871183; fax: +49 30 83856664.
E-mail address: luis.guanter@wew.fu-berlin.de (L. Guanter).

0034-4257/$ – see front matter © 2013 Published by Elsevier Inc.
http://dx.doi.org/10.1016/j.rse.2013.01.017

2008; Amorós-López et al., 2008; Corp et al., 2006; Damm et al., 2011; Daumard et al., 2010; Moya et al., 2004; Plascyk & Gabriel, 1975; Rascher et al., 2009; Zarco-Tejada et al., 2009, 2012), generally consisting in a measurement channel inside the O_2A-band and two reference channels located outside the absorption.

In the last years, spectro-radiometers with a sub-nanometer spectral resolution providing several measurements inside the O_2A- and O_2B-bands have enabled the application of the so-called spectral fitting methods (SFMs) (Meroni & Colombo, 2006; Meroni et al., 2010). In both cases, the *in-filling* of the O_2A- and O_2B-bands (centered around 760 nm and 687 nm, respectively) by F_s is determined by comparison with a reference measurement of the solar irradiance arriving at the canopy. To avoid confusion, it must be noted that the FLD method was originally developed for measurements in solar Fraunhofer lines (Plascyk & Gabriel, 1975), but it is being used with telluric O_2 bands for field-based F_s retrieval.

Both FLD and SFM techniques have been successfully used to retrieve F_s in O_2 absorptions from ground measurements (Amorós-López et al., 2008; Meroni et al., 2008, 2011; Middleton et al., 2008). However, the application of O_2A-based methods on airborne and spaceborne instruments is not straightforward due to the absorption of the F_s signal by O_2 between the surface and the top-of-atmosphere (TOA) and to the relatively strong impact of atmospheric scattering on the O_2 absorption features (Frankenberg et al., 2011a; Guanter et al., 2010). Satellite data have been successfully employed for O_2A-based retrieval of F_s from space, although only over some particular areas containing non-fluorescent surfaces to constrain the retrieval (Guanter et al., 2007). Methods for the retrieval of F_s from space-borne spectrally-resolved measurements in O_2A and O_2B are being investigated (Guanter et al., 2010) in the framework of the FLEX mission concept (Drusch & FLEX Team, 2008) currently under development within the 8th ESA Earth Explorer Program.

The high spectral resolution measurements provided by the Fourier Transform Spectrometer (FTS) onboard the Greenhouse gases Observing SATellite "IBUKI" (GOSAT) (Kuze et al., 2009) represent the first space data from which the production of global F_s maps has been feasible to date. The band 1 of the FTS covers the 756–775 nm spectral window with a spectral resolution of around 0.025 nm at 760 nm. This high spectral resolution has enabled the application of the F_s *in-filling* approach to individual solar Fraunhofer lines located around the O_2A-band. Different spectral components of the TOA signal are shown in Fig. 1 for a spectral resolution of around 0.13 nm. The 756–775 nm window covered by the GOSAT-FTS band 1 is in the center of the top-of-canopy radiance spectrum displayed. Both the O_2A-band and the Fraunhofer lines in the near-infrared region are shown. All the spectral features between 745 and 759 nm in the reflected radiance spectrum are due to Fraunhofer lines. The fractional depth of Fraunhofer lines is practically not affected by atmospheric absorption or scattering, which makes F_s retrievals in this spectral window to be almost insensitive to atmospheric effects (Frankenberg et al., 2012). The same *in-filling* principle was later used by Joiner et al. (2012) for global F_s retrievals from SCIAMACHY (SCanning Imaging Absorption spectroMeter for Atmospheric CHartographY) measurements in the strong Fraunhofer line in 866 nm.

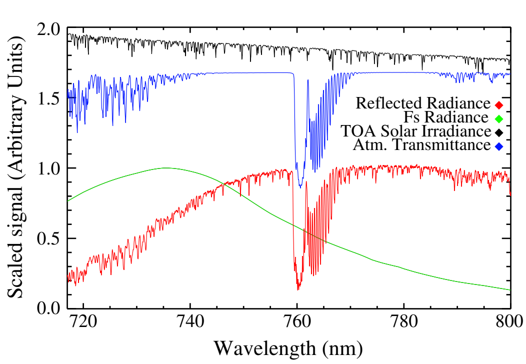

Fig. 1. Solar-reflected and fluorescence-emitted top-of-canopy radiance spectra compared with an extraterrestrial solar irradiance spectrum and an atmospheric transmittance spectrum. The reflected radiance spectrum is one of the OceanOptics HR4000 spectra used in this work. The solar irradiance and the transmittance spectra have been convolved with a spectral response function mimicking HR4000 measurements (spectral sampling of 0.02 nm and a full-width at half-maximum of 0.13 nm).

Here, we use top-of-canopy (TOC) radiance measurements to evaluate F_s retrieval methods applicable to space measurements. The main goals of this study are (i) to assess the potential of statistical F_s retrieval methods making use of broad fitting windows including both Fraunhofer lines and atmospheric bands, and (ii) to provide an indirect test of the consistency of Fraunhofer-line based F_s retrievals from space.

2. Materials and methods

2.1. Generalities on F_s retrieval

The spectral radiance measured by a sensor at the TOA over a fluorescent target with a reflectance assumed to be Lambertian can be formulated as

$$L_{\mathrm{TOA}} = L_0 + \frac{[E g \frac{\rho_s}{\pi} + F_s] T_{\uparrow}}{1 - S\rho_s}, \tag{1}$$

where ρ_s is the surface reflectance, L_0 is the atmospheric path radiance, E_g is the global (direct plus diffuse) at-surface irradiance, S is the atmospheric spherical albedo, and $T_{\uparrow}$ is the total atmospheric transmittance (for diffuse plus direct radiation) in the observation direction.

Assuming that $S\rho_s \ll 1$ in the near-infrared spectral window, and separating the solar-reflected and F_S terms, Eq. (1) can be written as

$$L_{\mathrm{TOA}} \simeq \mu_s I_{sc} \left[\rho_0 + T_{\downarrow} T_{\uparrow} \frac{\rho_s}{\pi}\right] + F_s T_{\uparrow}, \tag{2}$$

where μ_s is the cosine of the sun zenith angle, *Isc* is the extraterrestrial solar irradiance, ρ_0 the atmospheric path reflectance and $T_{\downarrow}$ is the total atmospheric transmittance in the illumination direction. The equivalent of this equation for a target at the top-of-canopy level is

$$L_{\mathrm{TOC}} \simeq \mu_s I_{sc} T_{\downarrow} \frac{\rho_s}{\pi} + F_s, \tag{3}$$

where the terms corresponding to the atmospheric path reflectance and the upward transmittance have been removed.

As discussed previously, F_s retrieval by the modeling of the *in-filling* of spectral features by F_s is based on the evaluation of either the atmospheric O_2 bands (typically the O_2A), modeled here by the $T_{\downarrow}$ term, or on the solar Fraunhofer lines given by I_{sc}. The use of one or the other type of spectral feature is conditioned by the measurement set-up: the O_2A-band is much wider and deeper than the individual Fraunhofer lines, so measurements in O_2A can be performed at a coarser spectral resolution and can potentially provide a higher precision in the retrieval due to the larger fractional depth than the shallower Fraunhofer lines. For measurements at the ground level, the reference fractional depth (without F_s) of the O_2A lines is accurately provided by measurements from a reference panel. Retrievals in O_2A are then preferred for ground-based F_s retrieval, whereas measurements in Fraunhofer lines can enable a simpler and bias-free F_s retrieval from space thanks to the very low sensitivity to atmospheric scattering. Nevertheless, the random component of the single-retrieval error can be high if the instrument has no sufficient signal-to-noise ratio (SNR) and/or spectral resolution.

2.2. Fundamental basis of the SVD-based approach for ground-based F_s retrieval

A linear forward model (F) can be defined to invert F_s from L_{TOA} or L_{TOC} spectra. For the TOC case in Eq. (3), this forward model can be expressed as

$$F\left(a, F_s^{760}\right) = I_t \sum_{i=0}^{n_p} a_i \lambda^i + F_s^{760} h_F \tag{4}$$

where I_t corresponds to either I_{sc} or $I_{sc}T_{\downarrow}$ depending on whether the fitting windows contains only Fraunhofer lines or also atmospheric features, respectively; F_s^{760} is a scalar representing F_s at a reference wavelength, which has been taken to be 760 nm; h_F is a fixed spectral function which accounts for the spectral shape of F_s, and λ is the array of measurement wavelengths. The polynomial in λ represents the low spectral frequency contribution due to surface reflectance and the atmospheric continuum absorption. Assuming that h_F and I_t are known, the retrieval state vector consists of the polynomial coefficients a_i and F_s^{760}.

It must be noted that a perfect instrument spectral calibration is assumed in this forward model. Parameters to account for spectral shift, stretch and broadening should be included in the retrieval vector in the real case, which would make the modeling more complicated, and the inversion to involve an iterative approach to solve for non-linear dependencies in the spectral convolution operation (Frankenberg et al., 2011a). In addition, there are uncertainties in the I_t term if this is taken from external sources, and the instrument radiometric response is not perfectly known.

This has been considered in the retrieval model proposed in this work by adapting the statistical method for F_s retrieval from GOSAT-FTS data described in Guanter et al. (2012) to field spectro-radiometer measurements. In its GOSAT-FTS version, the method is based on a linear forward model producing top-of-atmosphere (TOA) radiance spectra in 2–3 nm-wide micro-windows containing several Fraunhofer lines. The forward model consists of a series of 4–5 spectral vectors representing the variability of the solar-reflected contribution, including the overall signal intensity and spectral shifts, plus an additive term accounting for F_s at the TOA. The basis of spectral vectors was derived by means of a singular vector decomposition (SVD) (Press et al., 2007) of the training set made of F_s-free spectra from non-vegetated areas.

The SVD-based retrieval in Guanter et al. (2012) has been modified in this work so that it is able to cope with low spectral frequency patterns in the input radiance spectra. These are expected for the broader spectral fitting windows sampled by field radiometers. In the 717–780 nm range, which roughly covers the entire red-edge region, the reflectance of green vegetation increases non-linearly with wavelength mostly due structural and biochemical properties (mainly leaf area index and chlorophyll absorption). To model these patterns, the first and second singular vectors carrying most of the information for the reconstruction of the F_s-free part of the spectrum are convolved with a polynomial accounting for low-frequency changes in the continuum. The resulting forward model can be written as

$$F\left(a, b, c, F_s^{760}\right) = \upsilon_1 \sum_{i=1}^{n_p} a_i \lambda^i + \upsilon_2 \sum_{i=1}^{n_p} b_i \lambda^i + \sum_{i=1}^{n_v} c_i \upsilon_i + F_s^{760} h_F, \tag{5}$$

where n_v is the number of singular vectors used to account for the high-frequency information, n_p is the degree of the polynomial reproducing the low frequency patterns, a, b and c are arrays of coefficients with dimension n_p, n_p and n_v, respectively, λ is the wavelength array of the input spectrum (dimension n_λ), and υ is the $n_\lambda \times n_v$ matrix of singular vectors. The resulting linear forward model can be inverted by means of standard least squares fitting. This least square fitting should be weighted by the measurement error in the case of an instrument concept generating multiplicative noise (e.g. prism- or grating-based spectrometers), whereas no weighting would be necessary for instruments affected by white noise (e.g. an FTS). The retrieval error covariance S_e is given by

$$S_e = \left(J^T S_0^{-1} J\right)^{-1}, \tag{6}$$

where S_0 is the measurement error covariance matrix and J is the Jacobian matrix formed by the $\lambda^j \upsilon_i$ and h_F terms.

The set of singular vectors υ_i used for the inversion of the forward model in Eq. (5) is generated by means of the singular vector decomposition of a subset of 25 reference panel measurements taken at different times during each campaign day. As in Guanter et al. (2012), a threshold of 0.04% on the percentage of the variance of the training set explained by each singular vector is used to select n_v. Typical values of n_v are between 4 and 8 for the measurements used in this study. On the other hand, a second-order polynomial ($n_p = 2$) has been found to be sufficient to describe the low frequency contribution in fitting windows <15 nm width, whereas higher order polynomials were applied for wider windows as it will be discussed in Section 3.1.

As an example, the first 6 singular vectors from the windows 745–759 nm (only containing Fraunhofer lines) and 717–780 nm (full spectral window of the instrument) are displayed in Fig. 2. The first singular vector carries most of the variance of the training set, and reproduces the relative spectral intensity of the at-sensor radiance. The different Fraunhofer lines are clearly visible in the 745–759 nm window. The second singular vector accounts for spectral shifts in the reference measurements along the day. The third and forth vectors in the 745–759 nm window capture a periodic low frequency signal in the spectra which is thought to be coming from the detector. This pattern appears also in the wider window. Higher-order vectors have a lower weight and are mostly reproducing noise. Apparently, no singular vector reproduces spectral features similar to that of F_s, so no interference between F_s^{760} and the rest of the state vector parameters is expected.

An important aspect to be remarked is that the forward model in Eq. (5) could be directly applied to space-based measurements in any spectral window free from atmospheric bands. The derivation of the singular vectors would be performed with non-fluorescent surfaces as in Guanter et al. (2012). However, it should be modified for its application to wider fitting windows containing atmospheric features. In this case, the $T_{\uparrow}$ term should be included in order to account for the absorption of F_s by atmospheric components (water vapor and oxygen in the near-infrared) between the canopy and the sensor. This would lead to a more complex forward model, since the singular vector decomposition of the training set would only give the total transmittance ($T_{\downarrow}T_{\uparrow}$), so $T_{\uparrow}$ would have to be derived from it, which would not allow for a linear forward model. We will restrict ourselves to ground-based measurements in this work.

2.3. Fraunhofer-line discriminator (FLD) and spectral fitting methods (SFMs) for ground-based F_s retrieval in the O_2A-band

F_s has also been estimated with two state-of-the-art methods for on-ground measurements are used: FLD introduced by Plascyk and Gabriel (1975) and SFM proposed by Meroni and Colombo (2006). Both of these methods are designed to decouple F_s and ρ_s from L_{TOC} measurements as modeled by Eq. (3). To solve this equation, the FLD method uses radiance measurements in two narrow spectral bands, one at the shoulder and the other one at the bottom of the O_2A-band. Fluorescence is then computed by the determined linear system formed with Eq. (3) evaluated at these two wavelengths, on

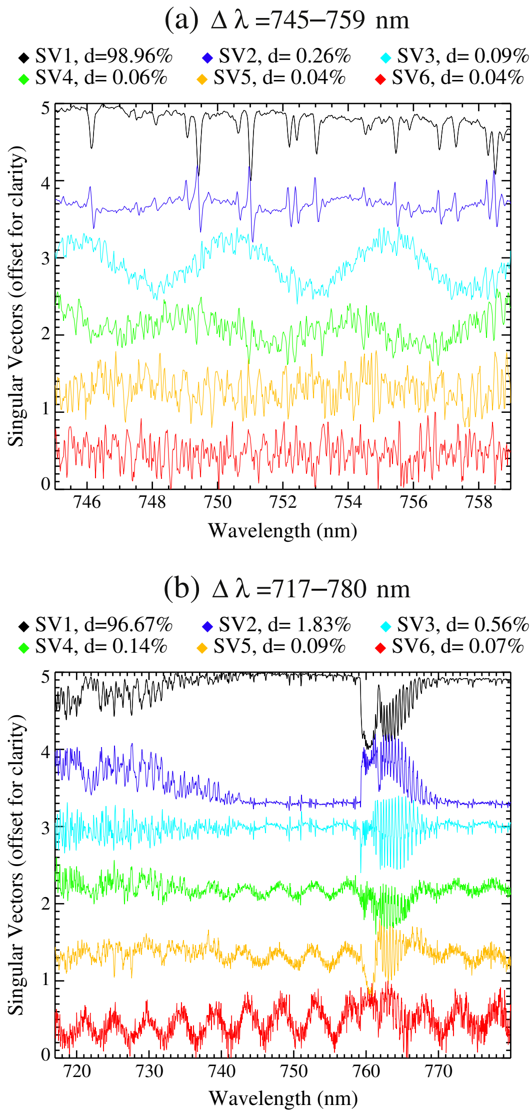

Fig. 2. First 6 singular vectors v_i from the singular vector decomposition of reference panel measurements in both the 745–759 nm and 717–780 spectral ranges. The percentage of the total variance of the training set represented by each singular vector is also displayed.

the assumption that the fluorescence flux and the reflection coefficient are spectrally constant. Wavelengths used in this work are 760.6 nm for the bottom and 759.2 nm for the shoulder of the O_2A-band as suggested in Meroni et al. (2010).

With SFMs, both F_s and ρ_s are determined employing mathematical functions to model the spectral shapes of F_s and ρ_s in the O_2A-band region. In this study, F_s and ρ_s have been modelled with linear functions in a restricted spectral range around the O_2A-band. With a large number of contiguous spectral observations provided by very high spectral resolution spectrometers (e.g. 0.1 nm bandwidth), an overdetermined bilinear system is formed with Eq. (3) and the four unknowns (i.e. gain and offset of the linear ρ_s and F_s functions) are estimated. The spectral interval used for F_s estimation is set to 759.00–767.76 nm, which leads to a total of 439 spectral channels for the spectro-radiometer used in this work.

The F_s estimates from the SFM are used as a reference in this study. Apart from the fact that this is a well tested method for ground-based F_s retrievals, each retrieval is performed through the normalization of the top-of-canopy radiance with an almost-simultaneous measurement of the downwelling irradiance. In this sense, it can be assumed that the SFM retrievals in this work are done under a perfect characterization of the atmospheric state and instrument performance so that the only task for the retrieval is to disentangle F_s and reflectance. In the case of the SVD approach, however, the weights of the atmospheric, reflectance, fluorescence and instrument contributions are free parameters in the inversion. This approach can therefore be thought of as a retrieval set-up closer to that of space-based observations for which no perfect knowledge of the down-welling irradiance is available to constrain the retrieval.

Related to this consideration of the SFM as the reference to assess the SVD retrievals, it must also be stated that the retrieval with the SFM can present errors such as those from a bad characterization of the surface reflectance or from unaccounted directional effects: the different contributions of direct and diffuse irradiance to the radiation reflected by either the canopy or reference panel measurement could lead to spurious in-filling of the O_2A-band which could propagate to biases in the estimated F_s. These potential impacts of directional effects on ground-based F_s retrieval have not been addressed by any study to the best of our knowledge. However, we will assume that the SFM constrained by simultaneous canopy and reference panel measurement is the best set-up for ground-based F_s retrievals.

2.4. Fitting windows considered for the SVD-based approach

The described SVD-based F_s retrieval approach has been tested on four different fitting windows in this study:

1. Fraunhofer lines, 745–759 nm: this is the widest window sampled in the near-infrared without the interference of atmospheric features (see Fig. 1).
2. Red-edge, 717–759 nm: it samples the Fraunhofer lines in the 745–759 nm range and some water vapor absorption bands between 717 and 745 nm.
3. O_2A-band, 745–780 nm: it samples the Fraunhofer lines in the 745–759 nm range and the entire O_2A-band between 759 and 780 nm.
4. Full-range, 717–780 nm: it is the widest fitting window provided by the instrument; it covers the Fraunhofer lines in the 745–759 nm range, the water vapor bands in 717–745 nm and the entire O_2A-band between 759 and 780 nm.

The first case represents a pure Fraunhofer-line F_s retrieval in which there is no interference with atmospheric absorptions features. A second-order polynomial is sufficient for the modeling of surface reflectance in the 745–759 nm window, but the retrievals are expected to be noisy because of the relatively low number of spectral channels and the fact that the fractional depth of the Fraunhofer lines is smaller than that of the atmospheric features. Concerning the other three cases, the water vapor or oxygen atmospheric features may have the role of Fraunhofer lines for F_s retrieval if the absorption between the canopy and the sensor is neglected. This applies to ground-based measurements, but would not be the case of an elevated. Having these broad spectral fitting windows enables us to minimize the impact of instrumental noise, although it renders the fit of the entire spectrum more complicated because the forward model has to deal with the non-linear background reflectance and fluorescence patterns. The impact of different polynomial orders in the modeling of the surface reflectance and of the assumption of a fixed shape for the F_s emission spectrum in h_F will be discussed in Section 3.1.

2.5. Experimental data set

The study site is a rice (Oryza sativa L. var. japonica) paddy field (400 m × 700 m) located in Northern Italy (45°03′46.25 N, 8°40′

06.74 E, 88 m a.s.l.). Spectral data were collected on seven sampling dates between July 5th 2007 and September 5th, 2007. Diurnal cycles of radiance spectra were collected on the rice field under clear sky conditions using a portable spectrometer (HR4000, OceanOptics, USA) characterized by a 707–805 nm spectral range, a Full Width at Half Maximum (FWHM) of 0.13 nm, a spectral sampling interval (SSI) of 0.02 nm and SNR of about 300. Noise in the HR4000 measurements is assumed to be only multiplicative (photon-noise type) in this work. The spectrometer was housed in a Peltier thermally controlled box (model NT-16, Magapor, Zaragoza, Spain) keeping the internal temperature at 25 °C in order to reduce dark current drift. The spectrometer was spectrally and radiometrically calibrated before the field campaigns with known standards (LS-1-CAL calibrated tungsten halogen lamp and CAL-2000 mercury argon lamp, OceanOptics, USA). Measurements were acquired every 10 min from 8:30 to 18:30 local solar time using a bare fiber optic with an angular field of view of 25° to measure from nadir at a distance of 1 m a circular area of the canopy of 44.4 cm in diameter. The fiber was mounted on a horizontal rotating mast in order to observe alternatively the canopy and the white reference calibrated panel (Optopolymer GmbH, Germany) employed to estimate incident radiance.

Every acquisition session consisted in the consecutive collection of the following spectra: instrument dark current, radiance of the white reference panel, canopy radiance and radiance of the white reference panel. Integration time was optimized before each acquisition session in order to exploit the full dynamic range of the spectrometers in any illumination conditions. The radiance of the reference panel at the time of the canopy measurement was then estimated by linear interpolation. For every acquisition, 4 scans were averaged and stored as a single file. Spectral data were acquired and pre-processed with dedicated software (Meroni & Colombo, 2009). An example of top-of-canopy radiance spectra used in this study is shown in Fig. 1. Sample F_s, atmospheric transmittance and extraterrestrial irradiance spectra are also plotted for reference.

Further spectral measurements were contemporary acquired with a second HR4000 (Ocean Optics, USA) spectrometer covering the 400–1000 nm spectral range with a FWHM of 1.4 nm (Rossini et al., 2010). Top-of-canopy reflectance spectra acquired by this second spectrometer around solar-noon for the seven campaign days are displayed in Fig. 3. The change in the reflectance patterns along the campaign can be seen. The first 5 spectra correspond to vegetative or reproductive phenological stages, whereas the last two days show vegetation in a ripening state when chlorophyll content starts to decrease. This is reflected in the value of the normalized difference vegetation index (NDVI) calculated from each spectrum.

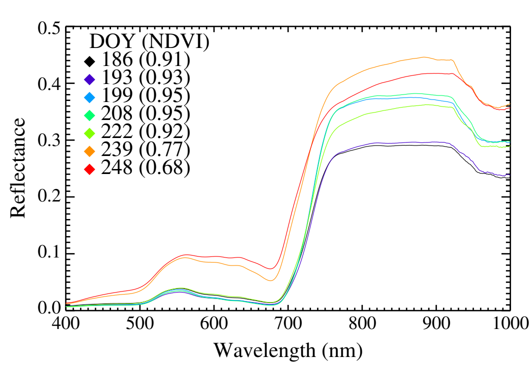

Fig. 3. Top-of-canopy surface reflectance spectra acquired by the wider-band spectrometer for the seven campaign days. The value of the normalized difference vegetation index (NDVI) calculated from each spectrum is displayed in the legend.

3. Results & discussion

3.1. Trade-off between spectral resolution and fitting window for F_s retrieval in the Fraunhofer lines

Firstly, we investigated the precision of F_s retrieval with the Fraunhofer line approach by means of a sensitivity analysis evaluating the impact of spectral resolution and width of the fit window on the retrieval. This analysis is useful to interpret our results and to further determine the best trade-off between resolution and spectral coverage for an instrument intended for ground-based retrievals in Fraunhofer lines.

Simulations were performed for a typical vegetation target in the 700–759 nm spectral window. A green vegetation reflectance spectrum from a spectral library was combined with a solar spectrum in order to generate a synthetic reflectance spectrum containing the Fraunhofer lines. Fluorescence was included as an additive term. A typical fluorescence spectrum with a peak intensity of 2.3 mWm^{-2} sr^{-1} nm^{-1} was used. The simulations were performed without considering the absorption by the water vapor bands in the 700–745 nm range, so only the pure in-filling of Fraunhofer lines without interaction with atmospheric features is evaluated. The SNR was taken to be of 300:1 at 757 nm, which is comparable to that of the HR4000 spectrometer used in this work, and only slightly higher than that of the GOSAT-FTS. This SNR figure is scaled for different signal levels assuming that noise is proportional to the square root of the input signal as it would correspond to shot-noise. Oversampling of 3 is assumed (i.e. 3 detector pixels per FWHM). No end-to-end simulation was performed for this analysis, but only the propagation of random noise to fluorescence retrievals for the different instrument configurations was investigated.

Results are depicted in Fig. 4. As expected, the retrieval precision depends strongly on both the measurement spectral resolution and fitting window. The two factors compensate each other for a given instrument configuration: the increase of the retrieval noise due to the loss of sensitivity associated to a coarser resolution can be counter-balanced by a broader fitting window. Also, the dependence of the retrieval noise on both parameters is highly non-linear (Fig. 4), which is explained by the positions of the Fraunhofer lines (sometimes an extension of the window includes new lines but sometimes it does not). For instance, in the case of a FWHM = 0.13 nm, a 10 nm increase of the fitting window for a width of 35 nm would have an effect about 10 times smaller than for a window of 10 nm. This kind of trade-off must be considered to assess the suitability of spectro-radiometers for F_s retrieval. In general, a higher spectral resolution is preferable to a wide spectral window: a higher spectral resolution combined with a narrower window can avoid atmospheric absorption features (as in the 745–759 nm window), and can also minimize the effect of the non-linear background reflectance and the shape of the F_s emission. The GOSAT-FTS configuration (fitting window width of around 3 nm, FWHM around 0.025 nm, typical SNR 150), not represented in the plot for visibility, leads to typical precision errors of 0.5–0.7 mWm^{-2} sr^{-1} nm^{-1} (Frankenberg et al., 2011b; Guanter et al., 2012).

3.2. Impact of reflectance and fluorescence modeling on broadband fluorescence retrievals

One of the main challenges for broadband F_s retrievals (as opposed to the relatively narrow 2–5 nm fitting windows used in GOSAT-FTS and SCIAMACHY retrievals) is to specify the spectral shape of surface reflectance and fluorescence in the forward model. A detailed theoretical study of the impact of reflectance and fluorescence modeling on SFMs can be found in Meroni et al. (2010). Here, we have performed further analysis of those effects for the SVD method based on the available set of real measurements.

The usual approach to model surface reflectance for F_s retrieval is to use polynomial functions which can adapt to all the possible

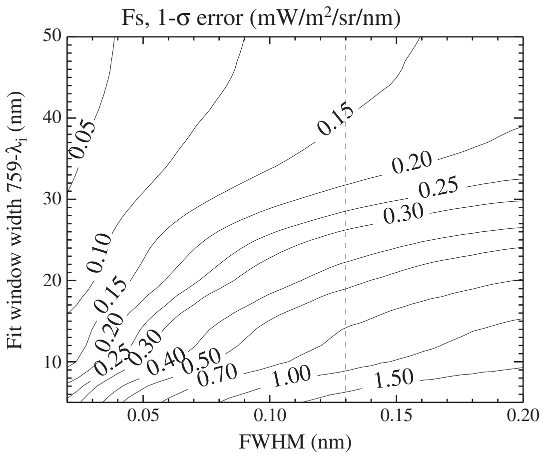

Fig. 4. Random error in F_s retrieval for a signal-to-noise ratio of 300 and different combinations of spectral resolution and fitting window width. The vertical dashed line marks the FWHM = 0.13 nm value of the HR4000 spectro-radiometer.

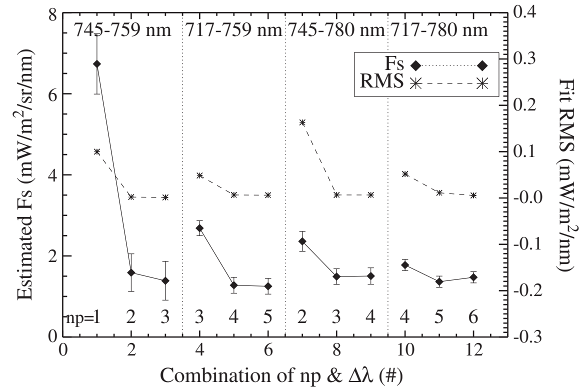

Fig. 5. Impact of the polynomial modeling of the surface reflectance. Mean F_s values are estimated from the same set of radiance spectra for the 4 fitting windows (Δλ) and different values of the degree of the polynomial modeling reflectance (n_p). The standard deviation from each set of retrievals is depicted as error bars. The root mean square (RMS) of the fit is plotted for the same combinations of Δλ and n_p.

reflectance patterns over land surfaces, which might include vegetated and non-vegetated covers. This is also the approach selected for our forward model in Eq. (5). However, the selection of the optimal polynomial order can be a difficult task with an important impact on the retrieval accuracy and precision. As some sort of bias-versus-variance dilemma, the modeling with a low-order polynomial can be relatively robust against instrumental noise, but can give rise to systematic errors in the retrieval from bad representations of the actual reflectance patterns propagating to the estimated F_s. On the contrary, a high-order polynomial could be flexible enough to properly reproduce all the possible variability in reflectance patterns, but would lead to a much higher sensitivity to instrumental noise.

These considerations have been tested by running the retrieval over a given set of measurements for three polynomial degrees (specified by n_p in Eq. (5)) in each of the 4 fitting windows. The mean F_s and the fit root mean square (RMS) from all the retrievals are plotted in Fig. 5. The standard deviation in each set of F_s retrievals is shown as error bars. It can be observed that the estimated F_s is higher for the lowest polynomial degrees considered for each window, and becomes relatively stable for the two higher polynomial degrees. The same happens to the RMS characterizing the goodness-of-fit. In view of these results, we have selected the central n_p value in each fitting window, under the assumption that using a higher n_p would not have a significant impact on the fit but might lead to a higher sensitivity to instrumental noise from over-fitting. This leads to $n_p = 2$ for 745–759 nm, $n_p = 4$ for 717–759 nm, $n_p = 3$ for 745–780 nm, and $n_p = 5$ for 717–780 nm.

On the other hand, the spectral shape of fluorescence, specified by the h_F function, has been chosen to be fixed in the forward model in Eq. (5). However, it is known that not only the intensity of the F_s emission is highly sensitive to changes in the environmental conditions, but also the spectral shape of the emission itself can change as a function of plant species, canopy structure and air temperature (Buschmann, 2007; Fournier et al., 2012). For instance, this change of the emission spectrum may induce changes in the slope of the F_s spectrum in the 745–759 nm window. To test the impact of a constant F_s spectrum shape h_F on the forward model in Eq. (5), we have run the retrieval in the four fitting windows over a set of real TOC radiance spectra changing h_F to slightly different F_s-like shapes (changes up to 3 nm in both center and width) simulating the second peak of the F_s emission.

The 15 different h_F spectra (before normalization to 760 nm) and the retrieval results obtained are plotted in Fig. 6. As expected, the results show a very little impact on F_s^{760} for the 745–759 and 745–780 nm windows, whereas it becomes larger for the wider fitting windows. Surprisingly, the highest impact is not found for the widest fitting window of 717–780 nm, but for 717–759 nm. This might be explained by the fact that the second fluorescence peak is roughly centered in the 717–759 nm window, which could make the retrieval to become more sensitive to the exact peak position.

In any case, the relative impact of h_F in this exercise is below 8% in this worst case of the 717–759 nm window, and this decreases to less than 4% in the others, which suggests that the prescribed shape of the fluorescence spectrum is not the most important error source in broadband retrievals. This agrees with the findings from Fournier et al. (2012).

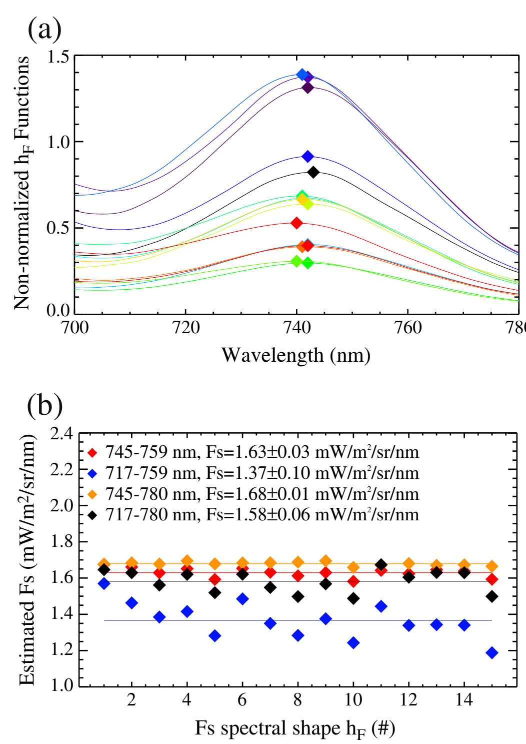

Fig. 6. Impact of the F_s spectral function (h_F) on the retrieval for the 4 fitting windows considered in this study. The 15 different h_F tested are plotted in (a), and the estimated F_s for all the h_Fs in (a) and the 4 fitting windows are plotted in (b). Mean and standard deviation from all 15 cases are displayed in the legend. The diamond symbols in (a) represent the maximum F_s for each h_F.

3.3. Forward model fits

Fig. 7 shows an example of the application of the SVD retrieval method described in Section 2 to the four spectral fitting windows extracted from the same at-sensor radiance spectrum. The fit of the forward model to the radiance spectrum in the 745–759 nm case is displayed in the top panel of Fig. 7(a). The spectral residual is shown in the center panel for both the original forward model and for the forward model without accounting for F_s. Small spectral differences can be observed at the location of Fraunhofer lines, which is further illustrated in the bottom panel depicting the difference between the fits with and without F_s. The retrieved F_s value and the estimated error (instrumental noise propagated to F_s with Eq. (6)) are also displayed. For this spectral fitting window, the forward model consists of the first 5 singular vectors of the set displayed in Fig. 2 plus a second-order polynomial to account for low-frequency background patterns.

A value of $F_s = (1.6 \pm 0.5)$ mWm^{-2} sr^{-1} nm^{-1} is retrieved from the fit in Fig. 7(a). The 1-σ error (derived from Eq. (6)) is about 30% of the F_s value in this particular retrieval. This single-retrieval error is comparable to the one reported in Frankenberg et al. (2011b) and in Guanter et al. (2012) for GOSAT-FTS retrievals, and is also comparable to the precision error estimated in Fig. 4. Despite the different resolution and fit window width of HR4000 and GOSAT-FTS, the validity of the estimation of F_s from GOSAT-FTS spectra through the evaluation of the *in-filling* of Fraunhofer lines by F_s is well illustrated by these field measurements.

Further investigation of the retrieval properties has been done with the wider spectral fitting windows. The fit of the forward model to the 717–759 nm, 745–780 nm, and 717–780 nm spectral windows is displayed in the other subfigures of Fig. 7. The good performance of the SVD-based approach to adapt to a wider spectral window can be stated. It must be remarked that the spectral range between 717 and 745 nm is affected by water vapor bands (see Fig. 1), which are being properly modeled by the forward model. The same is true for the O_2A-band in the 759–780 nm window. It is observed how the retrieved F_s values are $F_s = (1.3 \pm 0.2)$ mWm^{-2} sr^{-1} nm^{-1}, $F_s = (1.9 \pm 0.2)$ mWm^{-2} sr^{-1} nm^{-1} and $F_s = (1.8 \pm 0.1)$ mWm^{-2} sr^{-1} nm^{-1} for the 717–759 nm, 745–780 nm and 717–780 nm windows, respectively. The differences in the F_s estimates with these wider windows are up to 30% of a mean value of 1.5 mWm^{-2} sr^{-1} nm^{-1}, which is not explained by the smaller 1-σ random error estimate. It can be the case that the 1-σ error is underestimated in both cases, or that the retrieval is biased by potential dependencies on the modeling of reflectance and fluorescence patterns in the forward model, which would affect this wider fitting windows the most. On the other hand, it must also be noted that the 1-σ decreases as expected for the wider fitting windows with respect to the 745–759 nm window.

The difference of the fits with and without F_s in the third panel of Fig. 7(a)–(d) shows the *in-filling* of Fraunhofer lines and atmospheric bands. This is especially clear in the Fraunhofer line case in Fig. 7(a), and to some extent also in the first part of the spectrum (717–745 nm).

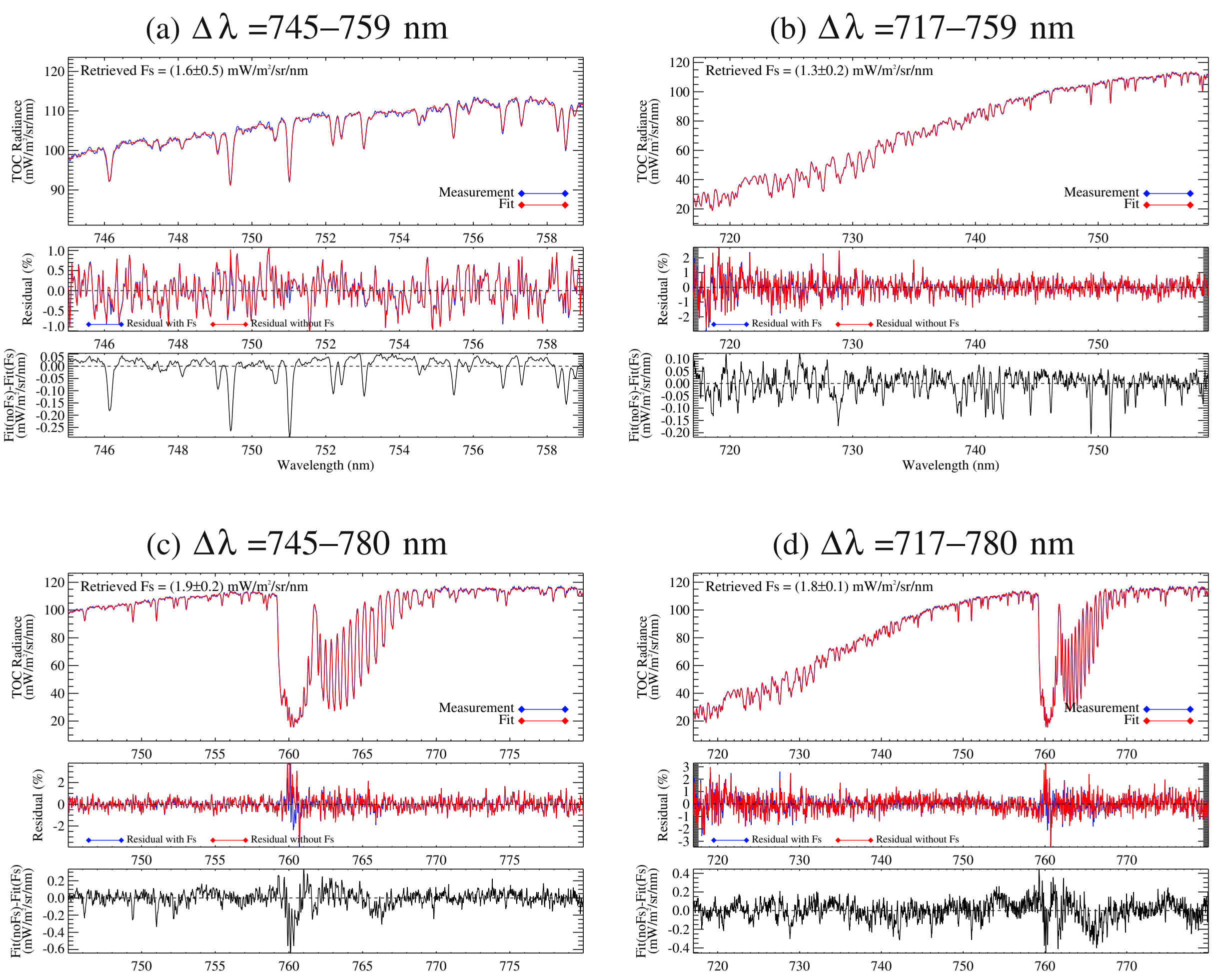

Fig. 7. Forward model fits for the 4 fitting windows considered in this study. The measurement and the fit of the forward model in Eq. (5) are plotted in the top panel of each subfigure. The spectral residual from the fit of the forward model both with and without considering F_s are displayed in the center panel. The difference between the fit performed with and without F_s in the forward model is shown in the bottom panel to illustrate the *in-filling* of Fraunhofer lines by F_s.

A careful comparison with the extraterrestrial irradiance spectrum in Fig. 1 shows that there is correlation between the strongest Fraunhofer lines (e.g. at 721 and 729 nm) and the negative spectral features in the residual difference plot.

Concerning the fits in the 759–780 nm window, the amplitude of the residual appears to be within the noise level. The higher residual in the bottom of the O_2A-band is explained by the fact that it is plotted in relative terms, as the absolute residual in those wavelengths follows the same noise-like patterns as in the rest of the spectrum. The in-filling of the Fraunhofer lines in the 745–755 nm region and in the O_2A-band around 760.5 nm can be observed in the difference between radiance modeled with and without F_s in the state vector. It could be hypothesized that such a small fit residual cannot be achieved with a physically-based approach due to the very complicated modeling of the atmospheric radiative transfer in O_2A and potential instrumental issues not considered in the forward model.

3.4. Comparison of SVD-based F_s retrievals with the FLD and SFM in O_2A

Next we compare the diurnal cycles of F_s as derived with the SVD-based method and the O_2A-based SFM and FLD techniques. The diurnal cycle of F_s as retrieved with the three approaches (745–759 nm and 717–759 nm fitting windows in the SVD-based case) is shown in Fig. 8. The down-welling radiance at 750 nm measured at the canopy level are also plotted. A high correlation between F_s and the down-welling radiance is detected as expected for green, non-stressed vegetation, which was the case on DOY 208.

It can be seen in Fig. 8 that the SVD-based retrievals in the 745–759 nm window are much noisier than the O_2A ones, although the general trend of the diurnal cycle is captured properly. This is explained by the fact that the fractional depth of Fraunhofer lines is much smaller than that of the O_2A-band in this spectral configuration, which makes the retrieval in Fraunhofer lines much more sensitive to instrumental noise. Also, it must be emphasized that the SVD method is based on a multi-parameter inversion approach which makes use of SVs calculated off-line from a subset of reference panel measurements, whereas the FLD and SFM have a perfect description of the atmospheric condition and the instrumental performance through the reference panel measurements used for each retrieval. It can also be noted that, as expected, the SFM using the O_2A-band is more robust against instrumental noise than the traditional FLD method due to the use of more measurement channels. The decrease of the F_s error for the wider window configuration is evident in the 717–759 nm plot. In this case, SVD retrievals are of comparable precision to those of O_2A-based methods due to the higher number of spectral features in the fitting window.

Scatter plots between SFM O_2A-based retrievals and the SVD method for the 4 fitting windows are displayed in Fig. 9. Each symbol represents the mean value calculated from all the measurements in the time period 10:00–15:00, and the error bars correspond to the standard deviation for the same set of retrievals, which is an indication of noise as well as of the diurnal variation of F_s. In general, the SVD-based retrievals match well those from the O_2-SFM, even for the pure Fraunhofer-line window 745–759 nm. The existence of fit slopes different from 1 and relatively high offsets can be explained by the small number of samples and the reduce range of variation. Assuming that the spectral fitting method in O_2A can be taken as the reference for ground-based F_s measurements for the reasons discussed previously in the text, the results in Fig. 9(a) can be considered as a first validation of the Fraunhofer-line principle for F_s retrievals. Furthermore, under the assumption that F_s retrievals from Fraunhofer lines in the 745–759 nm region are almost independent of atmospheric scattering (Frankenberg et al., 2012), these results also provide an indirect validation of F_s retrievals from GOSAT-FTS TOA spectra.

Concerning the other fitting windows, it can be observed that the error bars depicting the variability in the retrievals are much smaller

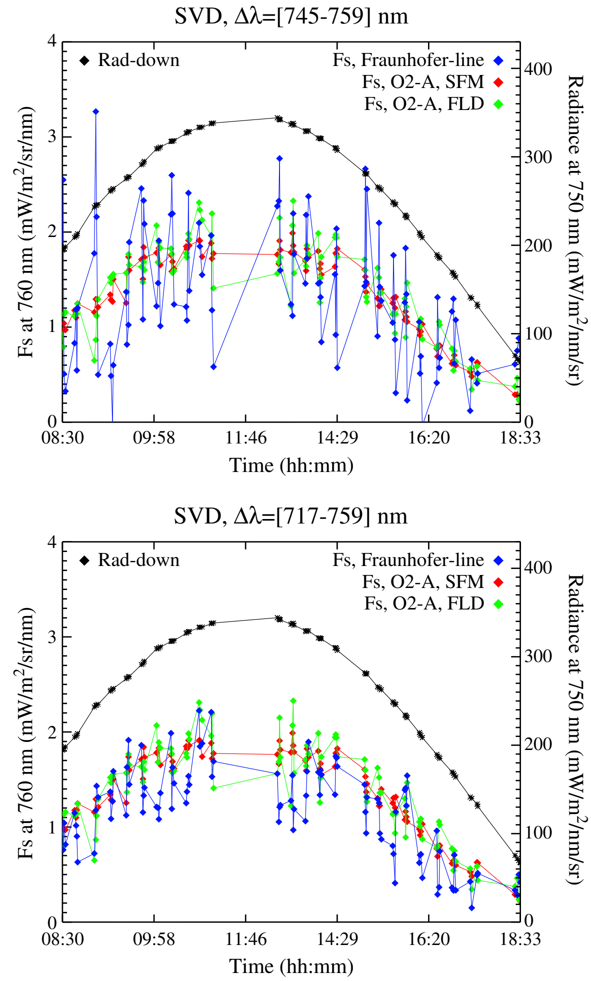

Fig. 8. Diurnal cycle of F_s on DOY 208 as calculated from the O_2A-band with FLD and SFM techniques and the SVD-based approach in 745–759 nm and 717–759 nm. The diurnal cycle of the down-welling sky radiance is also plotted. Samples between 11:00 and 12:00 are missing because at that time was impossible to view the target from nadir without shadowing it with the measurement system.

than for the pure Fraunhofer line case. A significant gain is found for the two fitting windows sampling the O_2A-band at 760 nm. This might be due to the O_2A-band being much deeper than the Fraunhofer lines, which provides a larger change of the fractional depth by F_s in-filling. This finding might not apply to the space-based case due to the absorption of F_s by the oxygen column between the canopy and the TOA. The retrievals in 717–759 nm appear to be biased by about 0.2 $mWm^{-2}\,sr^{-1}\,nm^{-1}$ with respect to the other fitting windows and the O_2A-SFM measurements, which can be partly explained by the dependency on the h_F shown in Fig. 6.

4. Summary and conclusions

We have used field spectroscopy to assess the potential of a statistical approach for the retrieval of sun-induced chlorophyll fluorescence from ground and space measurements. The proposed method relies on the modeling of the radiance spectra measured over the canopy with a set of spectral functions derived from non-fluorescent targets. Such spectral functions are produced with a singular vector decomposition technique applied to measurements over non-fluorescent targets. The resulting singular vectors are expected to describe the spectral variability in the radiance spectra except for that due to F_s. An earlier version of this SVD-based approach was used for space-based F_s retrieval from GOSAT-FTS data (Guanter et al., 2012). The GOSAT-FTS version of the method has been adapted so that it can be applied to broader fitting

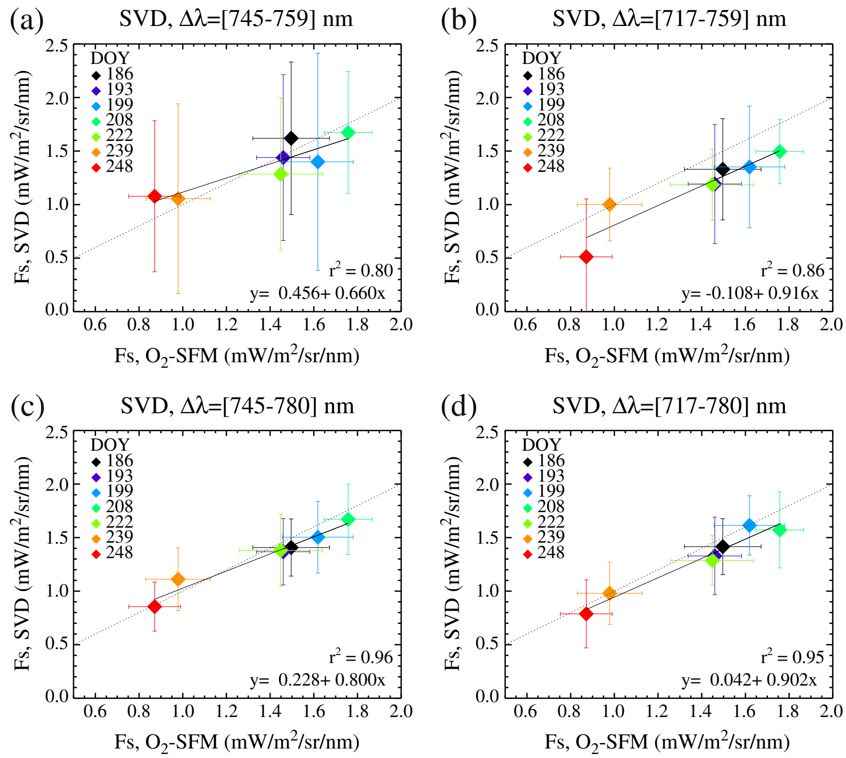

Fig. 9. Comparison between SFM-O_2A and SVD-based F_s retrievals. Diamond symbols and error bars depict the mean and standard deviation, respectively, from all the measurements between 10 h and 15 h of each day. The dotted line represents the 1:1 line. F_s is given at the reference wavelength of 760 nm.

windows as the ones provided by the HR4000 field spectrometer used in this work. This has allowed the investigation of aspects related to space-based F_s retrievals in broad fitting windows with statistical approaches, such as the impact on the retrieval of the width of the fitting window and the formulations of reflectance and fluorescence, and also to gain further confidence on the feasibility of pure Fraunhofer-line-based retrievals from space.

The retrieval has been tested on 4 spectral fitting windows, namely 745–759 nm (only Fraunhofer lines), 717–759 nm (water vapor and Fraunhofer lines), 745–780 nm (O_2A-band and Fraunhofer lines), and 717–780 nm (water vapor, O_2A-band and Fraunhofer lines). The results from the 745–759 nm window confirm the feasibility of F_s retrievals solely based on Fraunhofer lines, as done with GOSAT-FTS. Since Fraunhofer-line retrievals have a low sensitivity to atmospheric scattering (Frankenberg et al., 2012), the results presented in this work at the ground level support the retrieval of F_s from space in Fraunhofer lines. The main limitation of the Fraunhofer-line retrievals in this work is the high sensitivity to instrumental noise for the relatively coarse spectral resolution of the HR4000 spectrometer. Precision errors about 30% have been found for the 745–759 nm fitting window containing only Fraunhofer lines. These errors could be greatly reduced by increasing the integration time of the instrument or by aggregating measurements at the expense of a lower temporal resolution.

As an alternative to pure Fraunhofer-line retrievals, the wider fitting windows have been shown to be very effective in increasing the retrieval signal-to-noise ratio. Accuracy and precision similar to the traditional O_2-based SFM retrievals have been achieved for the two wider fitting windows containing the O_2A-band, which can be explained by the fact that this band is deeper than the Fraunhofer-lines. However, this finding would not apply to TOA measurements due to the absorption of F_s by the oxygen column between the canopy and the sensor. In general, measurements in 745–759 nm with high SNR and spectral resolution are preferable to a wider spectral window with lower SNR or spectral resolution, because the modeling of reflectance and fluorescence in the forward model becomes more complicated in a broader fitting window. The narrower window would also be preferred for space-borne F_s retrievals because it makes it unnecessary the modeling of the water vapor absorption in the 717–745 nm range or the O_2 absorption around 760 nm.

On the other hand, it has been demonstrated that statistical approaches such as the SVD-based one presented in this work are a plausible option for existing and future space-borne spectrometers resolving the O_2A-band, which has been a topic of active research in the last years. The very accurate reconstruction of the O_2A-band by the SVD-based approach can be an alternative to complex and error-prone physically-based approaches attempting to solve the complicated radiative transfer between the atmosphere, the surface and the instrument. The potential advantage of these statistical approaches is that they can reduce the fit residual to the level at which the F_s signal becomes separable from noise and other signals in the measurement.

A major challenge for the design of F_s retrieval methods for broad fitting windows is the formulation of the surface reflectance in the retrieval. A very flexible reflectance model can lead to over-fit the F_s signal, whereas a model with a low flexibility might lead to spectral residuals in the fit propagating to biases in the retrieved F_s. Polynomials with degrees from 2 to 5 have been selected for the different fitting windows in this study with apparently good results. The selection of those numbers has been based on a sensitivity analysis evaluating the improvements in the fit of the forward model for the different polynomial degrees. However, some further sensitivity analysis seems necessary to consolidate the optimal configuration, especially for a potential space-based algorithm needing to deal with all type of reflectance patterns. A physically-based reflectance model involving the vegetation parameters characterizing the red-edge reflectance could be an attractive alternative. Even though such a model might have problems to deal with non-vegetated or mixed-surface pixels, they could lead to a consistent retrieval of F_s and e.g. chlorophyll content and leaf-area index provided that the relationships between those parameters are properly constructed in the model. This possibility will be investigated in future work.

It must be stated that the SVD approach presented in this work is not intended to replace the SFM and FLD currently used in ground-based experiments. The main objective of the proposed SVD-based approach is to investigate the potential and limitations of statistical approaches for space-based F_s retrievals. However, a possible advantage of the SVD-based approach for ground-based measurements with respect to methods using panel measurements is that the former could work without those panel measurements by simply acquiring spectra over any non-fluorescent target (e.g. bare soils). Also, the SVD-based approach could also work over long time periods without any reference measurement by making the training off-line from measurements over non-fluorescent targets during some days (e.g. at the beginning and at the end of the campaign). A stable instrument would be necessary in this case.

Acknowledgment

This research has been funded by the European Commission through the 7th Framework Marie Curie Actions Programme and the Emmy Noether Programme of the German Research Foundation. The authors thank Albert Porcar-Castell from the University of Helsinki for his comments on an earlier version of the manuscript. We acknowledge the staff of the Remote Sensing of Environmental Dynamic Laboratory, DISAT, UNIMIB (S. Cogliati, M. Migliavacca) for their support during the field campaigns.

References

Alonso, L., Gómez-Chova, L., Vila-Francés, J., Amorós-López, J., Guanter, L., Calpe, J., et al. (2008). Improved Fraunhofer line discrimination method for vegetation fluorescence quantification. *IEEE Geoscience and Remote Sensing Letters*, *5*, 620–624.

Amorós-López, J., Gómez-Chova, L., Vila-Francés, J., Alonso, L., Calpe, J., Moreno, J., et al. (2008). Evaluation of remote sensing of vegetation fluorescence by the analysis of diurnal cycles. *International Journal of Remote Sensing*, *29*, 5423–5436.

Baker, N. R. (2008). Chlorophyll fluorescence: A probe of photosynthesis in vivo. *Annual Review of Plant Biology*, *59*, 89–113.

Buschmann, C. (2007). Variability and application of the chlorophyll fluorescence emission ratio red/far-red of leaves. *Photosynthesis Research*, *92*, 261–271, http://dx.doi.org/10.1007/s11120-007-9187-8.

Corp, L. A., Middleton, E. M., McMurtrey, J. E., Campbell, P. K. E., & Butcher, L. M. (2006). Fluorescence sensing techniques for vegetation assessment. *Applied Optics*, *45*, 1023–1033.

Damm, A., Erler, A., Hillen, W., Meroni, M., Schaepman, M. E., Verhoef, W., et al. (2011). Modeling the impact of spectral sensor configurations on the FLD retrieval accuracy of sun-induced chlorophyll fluorescence. *Remote Sensing of Environment*, *115*(8), 1882–1892, http://dx.doi.org/10.1016/j.rse.2011.03.011.

Daumard, F., Champagne, S., Fournier, A., Goulas, Y., Ounis, A., Hanocq, J. -F., et al. (2010). A field platform for continuous measurement of canopy fluorescence. *IEEE Transactions on Geoscience and Remote Sensing*, *48*, 3358–3368.

Drusch, M., & FLEX Team (2008). *FLEX report for assessment, ESA SP-1313/4*. Noordwijk (The Netherlands): ESA–ESTEC.

Flexas, J., Escalona, J. M., Evain, S., GulÃ-as, J., Moya, I., Osmond, C. B., et al. (2002). Steady-state chlorophyll fluorescence (Fs) measurements as a tool to follow variations of net CO2 assimilation and stomatal conductance during water-stress in C3 plants. *Physiologia Plantarum*, *114*(2), 231–240, http://dx.doi.org/10.1034/j.1399-3054.2002.1140209.x.

Fournier, A., Daumard, F., Champagne, S., Ounis, A., Goulas, Y., & Moya, I. (2012). Effect of canopy structure on sun-induced chlorophyll fluorescence. *ISPRS Journal of Photogrammetry and Remote Sensing*, *68*, 112–120, http://dx.doi.org/10.1016/j.isprsjprs.2012.01.003.

Frankenberg, C., Butz, A., & Toon, G. C. (2011). Disentangling chlorophyll fluorescence from atmospheric scattering effects in O2A-band spectra of reflected sun-light. *Geophysical Research Letters*, *38*(L03), 801, http://dx.doi.org/10.1029/2010GL045896.

Frankenberg, C., Fisher, J. B., Worden, J., Badgley, G., Saatchi, S. S., Lee, J. -E., et al. (2011). New global observations of the terrestrial carbon cycle from GOSAT: Patterns of plant fluorescence with gross primary productivity. *Geophysical Research Letters*, *38*(L17), 706, http://dx.doi.org/10.1029/2011GL048738.

Frankenberg, C., O'Dell, C., Guanter, L., & McDuffie, J. (2012). Chlorophyll fluorescence remote sensing from space in scattering atmospheres: implications for its retrieval and interferences with atmospheric CO_2 retrievals. *Atmospheric Measurement Techniques Discussions*, *5*(2), 2487–2527.

Guanter, L., Alonso, L., Gómez-Chova, L., Amorós, J., Vila, J., & Moreno, J. (2007). Estimation of solar-induced vegetation fluorescence from space measurements. *Geophysical Research Letters*, *34*(L08), 401, http://dx.doi.org/10.1029/2007GL029289.

Guanter, L., Alonso, L., Gómez-Chova, L., Meroni, M., Preusker, R., Fischer, J., et al. (2010). Developments for vegetation fluorescence retrieval from spaceborne high-resolution spectrometry in the O_2-A and O_2-B absorption bands. *Journal of Geophysical Research-Atmospheres*, *115*(D19), 303, http://dx.doi.org/10.1029/2009JD013716.

Guanter, L., Frankenberg, C., Dudhia, A., Lewis, P. E., Gómez-Dans, J., Kuze, A., et al. (2012). Retrieval and global assessment of terrestrial chlorophyll fluorescence from GOSAT space measurements. *Remote Sensing of Environment*, *121*, 236–251.

Joiner, J., Yoshida, Y., Vasilkov, A. P., Middleton, E. M., Campbell, P. K. E., Yoshida, Y., et al. (2012). Filling-in of near-infrared solar lines by terrestrial fluorescence and other geophysical effects: simulations and space-based observations from SCIAMACHY and GOSAT. *Atmospheric Measurement Techniques*, *5*(4), 809–829, http://dx.doi.org/10.5194/amt-5-809-2012.

Joiner, J., Yoshida, Y., Vasilkov, A. P., Yoshida, Y., Corp, L. A., & Middleton, E. M. (2011). First observations of global and seasonal terrestrial chlorophyll fluorescence from space. *Biogeosciences*, *8*(3), 637–651.

Kuze, A., Suto, H., Nakajima, M., & Hamazaki, T. (2009). Thermal and near infrared sensor for carbon observation Fourier-transform spectrometer on the Greenhouse Gases Observing Satellite for greenhouse gases monitoring. *Applied Optics*, *48*, 6716–6733.

Meroni, M., Barducci, A., Cogliati, S., Castagnoli, F., Rossini, M., Busetto, L., et al. (2011). The HyperSpectral Irradiometer, a new instrument for long-term and unattended field spectroscopy measurements. *The Review of Scientific Instruments*, *82*(043106), 1–9.

Meroni, M., Busetto, L., Colombo, R., Guanter, L., Moreno, J., & Verhoef, W. (2010). Performance of spectral fitting methods for vegetation fluorescence quantification. *Remote Sensing of Environment*, *114*, 363–374.

Meroni, M., & Colombo, R. (2006). Leaf level detection of solar induced chlorophyll fluorescence by means of a subnanometer resolution spectroradiometer. *Remote Sensing of Environment*, *103*, 438–448.

Meroni, M., & Colombo, R. (2009). 3 s: A novel program for field spectroscopy. *Computers & Geosciences*, *35*(7), 1491–1496.

Meroni, M., Rossini, M., Guanter, L., Alonso, L., Rascher, U., Colombo, R., et al. (2009). Remote sensing of solar induced chlorophyll fluorescence: Review of methods and applications. *Remote Sensing of Environment*, *113*, 2037–2051.

Meroni, M., Rossini, M., Picchi, V., Panigada, C., Cogliati, S., Nali, C., et al. (2008). Assessing steady-state fluorescence and PRI from hyperspectral proximal sensing as early indicators of plant stress. *Sensors*, *8*, 1740–1754.

Middleton, E. M., Corp, L. A., & Campbell, P. K. E. (2008). Comparison of measurements and FluorMOD simulations for solar-induced chlorophyll fluorescence and reflectance of a corn crop under nitrogen treatments. *International Journal of Remote Sensing*, *29*, 5193–5213.

Moya, I., Camenen, L., Evain, S., Goulas, Y., Cerovic, Z. G., Latouche, G., et al. (2004). A new instrument for passive remote sensing: 1. measurements of sunlight-induced chlorophyll fluorescence. *Remote Sensing of Environment*, *91*, 186–197.

Plascyk, J. A., & Gabriel, F. C. (1975). The Fraunhofer line discriminator MKII — an airborne instrument for precise and standardized ecological luminescence measurement. *IEEE Transactions on Instrumentation and Measurement*, *IM-24*, 306–313.

Porcar-Castell, A. (2011). A high-resolution portrait of the annual dynamics of photochemical and non-photochemical quenching in needles of pinus sylvestris. *Physiologia Plantarum*, *143*(2), 139–153, http://dx.doi.org/10.1111/j.1399-3054.2011.01488.x.

Press, W. H., Teukolosky, S. A., Vetterling, W. T., & Flannery, B. P. (2007). *Numerical recipes: The art of scientific computing*, *vol. 3*, : Cambridge University Press (65-74 pp.).

Rascher, U., Agati, G., Alonso, L., Cecchi, G., Champagne, S., Colombo, R., et al. (2009). CEFLES2: the remote sensing component to quantify photosynthetic efficiency from the leaf to the region by measuring sun-induced fluorescence in the oxygen absorption bands. *Biogeosciences*, *6*(7), 1181–1198.

Rossini, M., Meroni, M., Migliavacca, M., Manca, G., Cogliati, S., Busetto, L., et al. (2010). High resolution field spectroscopy measurements for estimating gross ecosystem production in a rice field. *Agricultural and Forest Meteorology*, *150*(9), 1283–1296, http://dx.doi.org/10.1016/j.agrformet.2010.05.011.

Soukupová, J., Cséfalvay, L., Urban, O., Košvancová, M., Marek, M., Rascher, U., et al. (2008). Annual variation of the steady-state chlorophyll fluorescence emission of evergreen plants in temperate zone. *Functional Plant Biology*, *35*, 63–76.

Zarco-Tejada, P. J., Berni, J. A. J., Suárez, L., Sepulcre-Cantó, G., Morales, F., & Miller, J. (2009). Imaging chlorophyll fluorescence with an airborne narrow-band multispectral camera for vegetation stress detection. *Remote Sensing of Environment*, *113*(6), 1262–1275.

Zarco-Tejada, P. J., González-Dugo, V., & Berni, J. A. J. (2012). Fluorescence, temperature and narrow-band indices acquired from a uav platform for water stress detection using a micro-hyperspectral imager and a thermal camera. *Remote Sensing of Environment*, *117*, 322–337.